Model dependence of the properties of S_{11} baryon resonances

Alvin Kiswandhi* and Simon Capstick†
Department of Physics, Florida State University, Tallahassee, Florida 32306-4350, USA

Steven Dytman‡
Department of Physics and Astronomy, University of Pittsburgh, Pittsburgh, Pennsylvania 15260, USA
(Received 23 August 2003; published 26 February 2004)

The properties of baryon resonances are extracted from a complicated process of fitting sophisticated, empirical models to data. The reliability of this process comes from the quality of data and the robustness of the models employed. With the large amount of data coming from recent experiments, this is an excellent time for a study of the model dependence of this extraction process. A test case is chosen where many theoretical details of the model are required, the S_{11} partial wave. The properties of the two lowest N^* resonances in this partial wave are determined using various models of the resonant and nonresonant amplitudes.

DOI: 10.1103/PhysRevC.69.025205 PACS number(s): 14.20.Gk, 13.30.Eg, 13.75.Gx, 24.85.+p

I. INTRODUCTION

The problem of extracting baryon resonance parameters from observables measured in scattering experiments is of fundamental importance. In order to understand the relevant degrees of freedom at low energy and their interactions in the few dozen N^* states found to date, reliable and objective information on their properties extracted from data is required. Models of the baryon spectrum are usually compared to masses defined in terms of effective Breit-Wigner parameters. A more sensitive test of such models is the comparison of total widths and branching fractions to open channels of each resonance to those extracted from data. These quantities are also defined in terms of effective Breit-Wigner parameters, but in general show more sensitivity to the method used to fit the data. What is not commonly appreciated is the dependence of these resonance parameters on the method used to extract them from a fit to the data. For example, it is not uncommon to see such parameters referred to as "data" in the literature.

The primary goal of this paper is to examine the model dependence in this process in a carefully chosen test case, states in the S_{11} partial wave in πN. States in this partial wave have both significant physics interest and significant uncertainty in their parameters as reported by the Particle Data Group (PDG) in their Review of Particle Properties [10]. Most of the literature considers the lowest-energy resonance in this partial wave [$S_{11}(1535)$] as a three-quark state within the quark model [1]. However, the substantial branching fraction of $S_{11}(1535)$ to ηN has, given the small phase space available for this decay, led to the interpretation of this state as a meson-baryon molecule [2]. Lattice calculations of the masses of these states have recently been developed [3,4]. The calculations of both Refs. [3] and [4] are quenched, and find masses for $S_{11}(1535)$ similar to the values fit from experiment [10]. In addition, constituent quark models which describe these S_{11} resonances as (P-wave) orbital excitations with $J^P=1/2^-$ differ in their prediction of the amount of mixing between the two possible quark-spin states [5], because of different models of the short-distance interactions between the quarks. A comparison between partial widths calculated in a given model and those extracted from data can be used to determine the nature of these short-distance interactions. This makes the dependence of these partial widths on the method used to extract them from fits to data important, and relevant.

These important microscopic issues are unable to be settled with the uncertainty in the full and partial widths presently reported by the PDG, which vary widely among various studies. At one extreme, analyses of the πN elastic scattering data tend to give a full width of about 120 MeV for $S_{11}(1535)$, with πN as the dominant decay branch [6,7]. At the other extreme, threshold eta photoproduction data give a much larger full width $\Gamma \sim 210$ MeV, with ηN as the larger decay branch [8]. Only a unified treatment of all the data can provide a consistent picture.

The purpose of this paper is to examine the model dependence of S_{11} resonance parameters by extracting them from several fits to a single set of partial-wave amplitudes for $\pi N \to \pi N$ [6] and $\pi N \to \eta N$ [9] scattering in the S_{11} partial wave. These fits have different levels of sophistication in their description of the scattering matrix. The analysis of these channels in this partial wave is chosen because the proximity of two overlapping resonances [$S_{11}(1535)$ and $S_{11}(1650)$] and the ηN channel threshold makes it an interesting and nontrivial example. Differing treatments of the rescattering processes are a key difference among the models studied here and these effects should be most important near a threshold. Although the number of open channels is much larger than two, the two channels that have been chosen are the most important and account for 90% (1535) and about 80% (1650) of the decay width when all channels are included [10].

Breit-Wigner models can get good fits to single-channel data (e.g., $\pi N \to \eta N$ [11], $\gamma N \to \pi N$ [12]), but have nontrivial

*Electronic address: alvin@heisenberg.physics.fsu.edu
†Electronic address: capstick@phy.fsu.edu
‡Electronic address: dytman+@pitt.edu

uncertainties and at times surprising results. In simplifying an intrinsically multichannel problem into a single-channel model, information from other reactions must be included with accompanying uncertainties. In addition, there is no single commonly accepted form for the resonance shape. When a somewhat large ($\sim$10) set of asymptotic states can couple to each N^* with high probability, including a large sample of reactions and application of the unitarity constraint are extremely important. Common multichannel techniques include *K*-matrix [13,14] and Carnegie-Mellon Berkeley (CMB) [9,15] models. Each has an established way of including a variety of interactions respecting multichannel unitarity with varying ability to include dynamics.

Three methods are used here to perform the extraction of resonance parameters via a fit to the partial-wave amplitudes. The most constrained is the CMB model, which was developed [16] to describe πN elastic and inelastic scattering, and extended and modernized in Ref. [9]. This approach has multichannel unitarity, and the scattering matrix (a matrix in the space of channels) has the required analytic structure. Resonances are modeled as "bare" poles, which are "dressed" by coupling to the open asymptotic channels.

The second, simpler approach is to describe the unitary T matrix using a real symmetric K matrix, which is in turn written directly in terms of resonance parameters. This approach maintains multichannel unitarity, but does not satisfy analyticity constraints. The third, simplest approach is to build the T matrix directly from a sum of relativistic Breit-Wigner forms for the resonances. In this case, minimal constraints on the scattering amplitudes are available. Below $\pi\pi$ production threshold, the overall amplitude can be made unitary using Watson's theorem. However, the ηN channel must be included for a good description of the S_{11} partial wave, and only *ad hoc* methods [12] are available to accomplish this. The Breit-Wigner models used here are neither unitary nor analytic.

Nonresonant amplitudes must be added to account for scattering processes which do not involve s-channel N^* resonances. Although a fairly small set of diagrams describing nonresonant processes can be identified at lower total energy ($W\sim 1.3$ GeV), the set of possible diagrams grows rapidly as the total energy increases to 2.0 GeV. To date, no published work has included all the relevant diagrams. Empirical descriptions of the nonresonant amplitudes can be chosen since each resonance has a strong signal in at least one of the reactions studied, and most publications find the nonresonant amplitudes to be smaller than the resonant amplitudes. In addition, the most basic physics assumption is that the resonances come from the long-distance part of the interaction and are seen in the sharp energy features of the data, while the nonresonant amplitudes arise from the short-range part of the interaction and provide smooth energy dependence. This implies that, in this case, the influence of the choice of nonresonant amplitudes on the extracted resonance properties should be small. The "distant-poles" model of the nonresonant amplitudes is designed for use with the CMB model. Bare poles well below and well above the thresholds for the channels being studied, i.e., distant poles, are fit to the partial-wave data with methods very similar to those used for the resonance poles. In the CMB model they provide a smooth, analytic, unitary T matrix in the physical region; they can also be incorporated into a K-matrix model to provide a unitary scattering matrix. While the poles and cuts in the left-hand part of the complex s plane required by crossing symmetry are difficult to fully implement in the CMB model, their effects in the physical region can be simulated by a particular choice of strong form factor, and by the use of subthreshold poles. Another method adds to the resonant amplitude polynomials quadratic in the parameters $x_c=(s-s_{\mathrm{th},c})^{1/2}$ for each exit channel c, which can yield a unitary T matrix for the K-matrix approach.

The procedure used here is to calculate, using the CMB, K-matrix, and Breit-Wigner approaches, the matrix T_{ab} for scattering between the channels $\{a,b\}\in\{\pi N,\eta N\}$ in terms of a set of parameters describing the resonant and nonresonant amplitudes. Different treatments of the background are explored, giving a total of eight different models. A χ^2 statistic is minimized by varying these parameters to best fit the partial-wave amplitudes for the $\pi N\rightarrow\pi N$ [6] and $\pi N\rightarrow\eta N$ [9] reactions.

The goals of this work are somewhat limited in order to make a clear statement about model dependence, and for this reason the resonance parameters which result should not be considered for use in understanding the microscopic structure of the S_{11} resonance states. The channel space is greatly simplified to only the two principal channels, leaving out other channels such as $\pi\Delta$ that are a much smaller part of the amplitudes, but which must be included for the optimal values. From ten-channel fits to both πN and γN reactions, the $S_{11}(1650)$ width is known to be $\sim$50 % larger than in a two-channel fit. In addition, the sophisticated K-matrix techniques developed by the Giessen group [13] are not used here.

II. MODELS OF THE SCATTERING MATRIX

In this section the form of the scattering matrix in the various models is described, along with the implementation of the two forms of background described above. All of the models used here require partial-wave amplitudes (PWA) as input. These extract the energy dependence of amplitudes with specific isospin, parity, and angular momentum (e.g., S_{11}) from the large number of experimental data points. About 20 years ago, significant efforts were made to find model independent methods for partial-wave analysis of πN elastic data [7]. More recent efforts by the George Washington University (GWU) group [6] incorporate most of the theoretical constraints developed previously. Although the fits in this work do not use the most recent GWU work, results using the most recent PWA would not produce different conclusions. Since the number of data points for the $\pi N\rightarrow\eta N$ reaction is much smaller, there is more model dependence. These amplitudes are discussed in Ref. [9], using a method that accurately couples the πN elastic and inelastic data with minimal model dependence. Until another study is done, this is the only PWA result available for $\pi N\rightarrow\eta N$.

A. CMB model

In this work the S_{11} partial wave in πN elastic and $\pi N\rightarrow\eta N$ scattering is described using only the two light reso-

nances $S_{11}(1535)$ and $S_{11}(1650)$. In the CMB model background (t- and u-channel) processes are simulated using one high-energy and two subthreshold s-channel poles, which are treated identically to the resonances in order to preserve the analytic structure of the T matrix. The transition amplitudes [9,16] are

$$T_{ab} = \sum_{i=1}^{5}\sum_{j=1}^{5} f_a(s)\sqrt{\rho_a(s)}\,\gamma_{ai}G_{ij}(s)\,\gamma_{bk}\sqrt{\rho_b(s)}f_b(s), \qquad (1)$$

where $\{a,b\} \in \{\pi N, \eta N\}$ label the channels, and i,j label the poles, which can represent the resonances or the background. The model used in this paper has five poles (two for real resonances and three for background resonances). It is easy to add channels with this formalism if the input data are available. The phase-space factor $\rho_a(s)$ has the form

$$\rho_a(s) = \frac{p_a}{\sqrt{s}}, \qquad (2)$$

where p_a is the c.m. frame momentum and γ_{ai} is the real-valued coupling constant of resonance i to the channel a. The form factor f_a in Eq. (1) is unity in the S wave.

The dressed propagator $G_{ij}(s)$ allows resonance i to couple to resonance j through rescattering, and is the solution of the Dyson equation

$$G_{ij}(s) = G^0_{ij}(s) + G^0_{ik}(s)\Sigma_{kl}(s)G_{lj}(s). \qquad (3)$$

The bare propagator $G^0_{ij}(s)$ has the form

$$G^0_{ij}(s) = \frac{\delta_{ij}e_i}{s_{0i} - s}, \qquad (4)$$

where $e_i = +1$ for the resonances and the high-energy background pole, and s_{0i} is the bare mass of the resonance (background pole). One subthreshold pole has $e_i = +1$ (repulsive), and the other has $e_i = -1$ (attractive).

The self-energy Σ_{kl} in Eq. (3) is the sum over channels c,

$$\Sigma_{kl} = \sum_{c=1}^{2} \gamma_{ck}\phi_c(s)\gamma_{cl}, \qquad (5)$$

where $\phi_c(s)$ is the channel propagator, which plays a central role in the CMB model. The sum is over the two channels in this simplified problem. Two-pion channels such as ρN can be included by treating them as quasi-two-body channels, which results in an enlarged T matrix. The rescattering sum in Eq. (5) will then extend over the additional channels. The imaginary part of ϕ_c is the product of phase space, ρ_c(s), with the square of the form factor for channel c (this quantity will be seen in the other models below) and the real part is obtained through a once-subtracted dispersion integral [9,16]. The desired analyticity of the entire amplitude is then assured.

Unitarity comes about because of the democracy of the rescattering in the Dyson equation, Eq. (3). In the multichannel context, unitarity is expressed through a generalized optical theorem,

$$\mathrm{Im}\, T_{ab} = \sum_c T^*_{ac}T_{cb}. \qquad (6)$$

Unitarity is also related to the properties in the complex plane through the discontinuity in the amplitude across the right-hand cut.

The dressed propagator $G_{ij}(s)$ can be found by solving algebraically the matrix equation (3), with the result

$$H_{ij}(s) \equiv [G^{-1}(s)]_{ij} = [G^0(s)^{-1}]_{ij} - \Sigma_{ij}(s) = \frac{s_{0i} - s}{e_i}\delta_{ij} - \Sigma_{ij}(s), \qquad (7)$$

and the matrix $G(s)$ can be found by inverting $H(s)$. This completes the necessary ingredients for calculating the T matrix in the CMB model of Eq. (1) in terms of three parameters for each resonance or background pole. These are the bare mass squared $s_{0,i}$, and the coupling strengths $\gamma_{\pi N,i}$ and $\gamma_{\eta N,i}$. Since there are five poles, this model has a total of 15 parameters.

Once this T matrix is fitted to the partial-wave data by varying these 15 parameters, baryon resonance parameters are extracted from the resonant part of the T matrix. The procedure for doing this is described in what follows.

B. Extraction of resonance parameters in the CMB model

Poles in the resonant part of the T matrix occur at complex values of s where the denominator of the resonance propagator vanishes. A search program finds these pole locations, and these are the model-free output (see Ref. [9] for details). This is possible because the amplitude has reasonable properties for complex values of s.

However, it is important to derive effective Breit-Wigner parameters for each resonance from this model. Once the pole positions are found, the matrix $H(s_{\mathrm{pole}})$ is diagonalized to eliminate interference between resonances. The denominator of the resonant part of the T matrix in the vicinity of each pole is then expanded in s. The constant term becomes the dispersive correction to the mass, and the term linear in s becomes the width of a generalized relativistic Breit-Wigner form. Thus, although the energy dependence of a resonance in the CMB model is much more sophisticated than the normal Breit-Wigner shape, all characteristics of a resonance can be expressed in this commonly used form.

C. CMB model with polynomial background

This is a modified CMB model which uses a polynomial function to describe the background. Care must be taken to maintain unitarity of the T matrix. Using a technique from Ref. [17], the full S matrix is written

$$S = B^{\dagger}RB, \qquad (8)$$

where R and B are the resonant and nonresonant S matrices, respectively. Here $R = I + 2iT$ uses the CMB-model T matrix, and B is a unitary matrix that need not be symmetric. The background matrix B is constructed from a real symmetric matrix K^B,

$$B = (1 + iK^B)(1 - iK^B)^{-1}, \tag{9}$$

where for the two-channel case of interest

$$K^B = \begin{bmatrix} k_{\pi\pi}x_\pi + k'_{\pi\pi}x_\pi^2 & k_{\pi\eta}x_\eta + k'_{\pi\eta}x_\eta^2 \\ k_{\pi\eta}x_\eta + k'_{\pi\eta}x_\eta^2 & k_{\eta\eta}x_\eta + k'_{\eta\eta}x_\eta^2 \end{bmatrix}, \tag{10}$$

or

$$K^B_{ab} = k_{ab}x_b + k'_{ab}x_b^2, \tag{11}$$

$x_b = \sqrt{s-(m_N+m_b)^2}$ for s above exit channel threshold and zero otherwise, and the coefficients k_{ab} and k'_{ab} are real. Note that the off-diagonal terms in K^B are zero for s below ηN threshold. This ensures that the diagonal and off-diagonal elements of R are not mixed, so the $\pi N \to \eta N$ amplitude vanishes below ηN threshold. This model has six real parameters describing the background, and six describing the resonances, for a total of 12 real parameters.

Once the S matrix in Eq. (8) is formed, it can be easily converted using $S = I + 2iT$ to a T matrix that can be fit to the partial-wave amplitudes by varying these 12 parameters in the usual way, and the extraction of the baryon parameters is identical to that of the original CMB model.

D. *K*-matrix models

A unitary S matrix can be constructed from a real, symmetric K matrix via $T = K(1 - iK)^{-1}$. This method is very common in the literature [13,18–20] for investigating hadrons in reactions. Recently, effective Lagrangian models [13] have been used with a K matrix for studies of N^* states. Nonrelativistic reductions of Feynman diagrams make these studies more sophisticated than what is presented here. The earlier work of Moorhouse and collaborators [19] is very similar to the method used here.

The differences between the CMB and K-matrix models are well known. A common problem with all K-matrix methods is the difficulty in maintaining analyticity. Only the work of Longacre [18] accomplished this. Thus, pole positions and residues can be obtained from the CMB fits and not from the K-matrix fits. Many researchers feel these values have less model dependence. Any microscopic model (e.g., lattice QCD) which has the analytic properties as an output can only use the CMB results. While the CMB model has a full treatment of rescattering, only the imaginary part of the channel propagator is included in the K-matrix model. The choice of the S_{11} resonances near ηN threshold as a test case is motivated by the expectation that these rescattering effects are most important close to threshold. As discussed above, the K-matrix method can be incorporated directly into an effective Lagrangian formulation [13]. As a result, the nonresonant amplitudes can be added diagram by diagram. This is a significant advantage over the present version of the CMB model, which is formulated in terms of amplitudes rather diagrams. In this work, we use the amplitude form of the K-matrix model [19,20].

Although the CMB model is preferred on theoretical grounds, the K-matrix model has practical advantages. It is more commonly used, and the less complicated treatment of interference and rescattering effects simplifies the fits to partial-wave amplitudes.

As in the CMB model, two subthreshold poles and one high-energy pole can be used to describe the nonresonant part of the scattering matrix. The contributions from the resonance and nonresonant poles are

$$K^i_{ab}(s) = \frac{\sqrt{\rho_a(s)}f_a(s)\gamma_{ai}\gamma_{bi}f_b(s)\sqrt{\rho_b(s)}}{(s_i - s)e_i}. \tag{12}$$

Here the form is similar on the surface to what is used in CMB model. The phase space $\rho_a(s)$ is given by Eq. (2), $f_a(s)$ is the form factor (none is needed for S wave), γ_{ai} is the coupling constant of the resonance or background pole i to channel a (but with units different from the CMB model), and s_i is the position of the ith (real) pole. The signs e_i are the same as those used in CMB model, with $e = +1$ for the resonances, the high-energy background pole, and one subthreshold background pole, while the second subthreshold background pole has $e = -1$. The K matrix is formed from a simple sum over the resonance and background poles,

$$K_{ab}(s) = \sum_{i \in \text{poles}} K^i_{ab}(s). \tag{13}$$

When the K matrix is converted to a T matrix, rescattering ("dressing" of the resonance) comes about naturally and the resonance gains a finite width. In this model the K matrix is written directly in terms of the resonance parameters, so that $M_i = \sqrt{s_i}$ is the mass of the resonance associated with the pole at s_i, the partial width of the ith resonance to channel a is

$$\Gamma_{ai} = \frac{\rho_a(s_i)f_a^2\gamma_{ai}^2}{M_i}, \tag{14}$$

and the total width is the sum of the partial widths. As discussed above, the differences between CMB and K-matrix formalism are seen only when interactions with other resonances and nonresonant amplitudes occur. These differences are expected to be maximized close to a channel threshold, which is the reason for the choice of the S_{11} partial wave with resonances near ηN threshold. In this case, the CMB model is expected to give more reliable results.

An alternate description of the background is using the polynomial form of Eq. (10), which is added to the resonance K matrix

$$K_{ab} = \sum_{i \in \text{resonances}} K^i_{ab}(s) + K^B_{ab}. \tag{15}$$

With either method of treating the background, these K-matrix models have the same total number of parameters as the CMB models, 15 for the distant-poles background and 12 for the polynomial background.

E. Breit-Wigner models

There are two kinds of Breit-Wigner model used here along with two kinds of nonresonant amplitude parametrization. In each model, the resonant and nonresonant T matrices are summed,

$$T_{ab}(s) = \sum_{i \in \text{resonances}} T^i_{ab,\text{res}}(s) + T_{ab,\text{nonres}}(s). \quad (16)$$

This form is inconsistent with unitarity without special effort.

The resonant amplitude $T^i_{ab,\text{res}}(s)$ is given by

$$T^i_{ab,\text{res}}(s) = \frac{\sqrt{\Gamma_{ai}\Gamma_{bi}}\sqrt{s}}{e_i(s_i - s) - i\sqrt{s}\Gamma_i} e^{i\theta^{ab}_i}. \quad (17)$$

The signs e_i are the same as in the CMB and *K*-matrix models, s_i is the pole position (with $M_i = \sqrt{s_i}$ for resonance poles), and $\Gamma_i = \Sigma_a \Gamma_{ai}$ is the total width of resonance *i*. Using a procedure similar to that of Ref. [12], an arbitrary phase $\exp(i\theta^{ab}_i)$ is associated with each pole in each channel. As shown below, the freedom to fit these additional phases is crucial to achieving a good fit with a Breit-Wigner model to the S_{11} partial-wave *T*-matrix elements in these channels.

The width commonly used to describe a nonrelativistic Breit-Wigner form is the energy-dependent width

$$\Gamma^{\text{n.r.}}_{ai}(s) = \Gamma_{ai}(s_i)\frac{\rho_a(s)}{\rho_a(s_i)}, \quad (18)$$

with the phase-space factor $\rho_a(s)$ as in Eq. (2). (Note that this is not the same as the conventional nonrelativistic Breit-Wigner energy dependence.) An alternative, relativistic form results from the assumption that the numerator of the contribution of resonance *i* to the *K* matrix in Eq. (12) is the same as that in the Breit-Wigner form in Eq. (17). If the partial width used in the *K*-matrix formalism, Eq. (14), is generalized to an energy-dependent function by replacing M_i with $\sqrt{s}$, then the *K*-matrix numerator of Eq. (12) is

$$\begin{aligned}\sqrt{\rho_a(s)} f_a(s)\gamma_{ai}\gamma_{bi}\sqrt{\rho_b(s)} f_b(s) &= (\Gamma_{ai}\sqrt{s})^{1/2}(\Gamma_{bi}\sqrt{s})^{1/2} \\ &= \sqrt{\Gamma_{ai}\Gamma_{bi}}\sqrt{s}, \end{aligned} \quad (19)$$

which is the same as the numerator in Eq. (17). This suggests the use of

$$\Gamma^{\text{rel}}_{ai}(s) = \Gamma_{ai}(s_i)\frac{\sqrt{s_i}}{\sqrt{s}}\frac{\rho_a(s)}{\rho_a(s_i)}, \quad (20)$$

for the energy-dependent partial width in a relativistic Breit-Wigner form. In what follows models using both $\Gamma^{\text{n.r.}}_{ai}(s)$, labeled $\text{BW}_{\text{n.r.}}$, and $\Gamma^{\text{rel}}_{ai}(s)$, labeled BW_{rel}, are used in fitting the Breit-Wigner form in Eq. (17) to the S_{11} partial-wave *T*-matrix elements, and the results are compared. The relativistic form is the same as that advocated by Chung *et al.* [20].

The first nonresonant form uses distant poles to describe the background contributions to the *T* matrix, so that the total *T* matrix is a simple sum

$$T_{ab}(s) = \sum_{i \in \text{poles}} T^i_{ab}(s). \quad (21)$$

This form of background has two low-energy poles and one high-energy pole, the same as was used with the CMB and *K*-matrix models. To get a good fit, each of these terms requires an additional phase in each channel, as described above. With the background described by distant poles, there are 15 parameters (mass, width, and πN branching fraction for each term) associated with the five poles, and ten phases, for a total of 25 real parameters. Of the models used in this work, this model has the largest number of parameters.

As with CMB and *K*-matrix models, it is possible to describe the nonresonant background by a polynomial function, so that

$$T_{ab}(s) = \sum_{i \in \text{resonances}} T^i_{ab,\text{res}}(s) + T_{ab,\text{nonres}}(s), \quad (22)$$

where the background *T*-matrix elements are the polynomials

$$T_{ab,\text{nonres}} = \kappa_{ab} x_b + \kappa'_{ab} x_b^2. \quad (23)$$

As with the other models, $x_b = \sqrt{s - (m_N + m_b)^2}$ for *s* above exit channel threshold and zero otherwise, but now the coefficients κ_{ab} and κ'_{ab} are complex. In this model there are six resonance parameters associated with the two poles, and eight background parameters (two complex numbers for each of two channels), for a total of 18 real parameters.

III. RESULTS

In order to understand the complications in the S_{11} partial wave, model predictions for a hypothetical isolated resonance are first considered. Figure 1 compares the results of all four models for the scattering amplitude of an isolated single-channel *S*-wave resonance. An *S*-wave resonance is chosen with a mass of 1710 MeV and width of 215 MeV in the $\pi N \to \eta N$ reaction, which avoids any complications with centrifugal barriers. Agreement among the different formulations is striking, despite the deliberate choice of a resonance mass close to ηN threshold. The *K*-matrix and CMB models have identical forms for an isolated resonance. The relativistic Breit-Wigner is chosen to be identical with the CMB model in this limit. Even the Breit-Wigner amplitude with the nonrelativistic width is in good agreement with the other forms. If the complex amplitudes are plotted on an Argand diagram (with the real part of the amplitude on the horizontal axis, and the imaginary part on the vertical axis), all will show the typical counterclockwise circular motion of a resonance. Nonresonant background will cause a shift or a distortion of this basic shape, and inelasticity will decrease the radius. Interference between resonances can have significant effects.

A partial-wave amplitude with this *W* dependence is the most visible signature of a resonance, producing a peak in the total cross section with an appropriate width. Such a peak is seen in the total cross section for $\pi N \to \eta N$, and is often interpreted as a resonance. The S_{11} partial-wave amplitude dominates the total cross section for this reaction, and is shown in the bottom two panels of Fig. 2. Since the higher mass resonance $S_{11}(1650)$ couples weakly to this channel, this appears to be an isolated resonance with small nonresonant amplitudes.

Single-channel fits of the $\pi N \to \eta N$ amplitudes have been

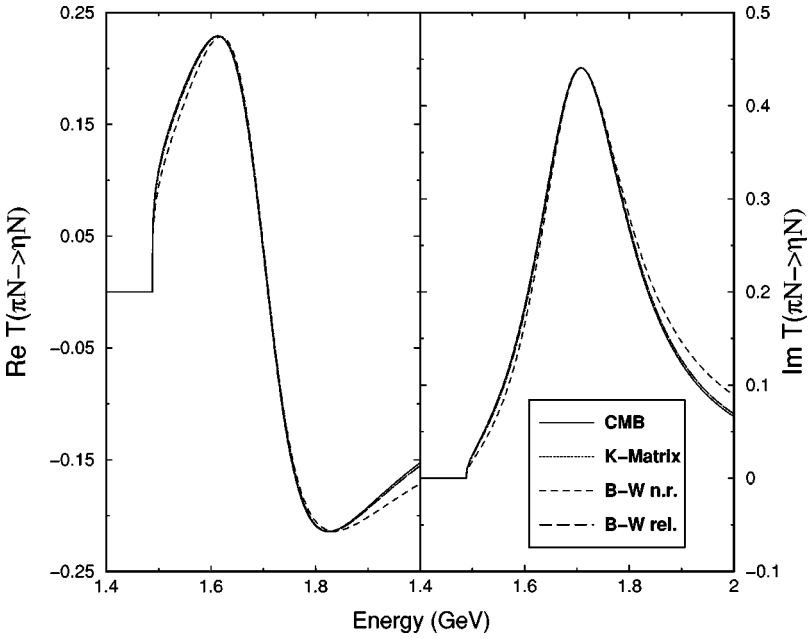

FIG. 1. Real parts (left panel) and imaginary parts (right panel) of $\pi N \to \eta N$ resonant scattering amplitudes calculated with an isolated S-wave resonance of mass 1710 MeV and width 215 MeV, in each of the four models used here.

made, which are shown as curves in the bottom two panels of Fig. 2. The results are similar to those of single-channel fits with a Breit-Wigner energy dependence to the total cross sections for $\pi^- p \to \eta n$ and $\gamma p \to \eta p$ [8]. The data can be fit using an S-wave Breit-Wigner form if a small, but important contribution from nonresonant amplitudes is included and the energy region used in the fit is truncated. This rough fit can be used to determine the product of the initial and final state couplings to the resonance, requiring information from more complete fits to account for the missing decay strength of the $S_{11}(1535)$ resonance to other channels. The single-channel, one-resonance fit shown in Fig. 2 is made with a Breit-Wigner resonant shape with the relativistic form of the width, the polynomial form of the background, and a single phase multiplying the resonant amplitude, truncating the fit at 1700 MeV. The result is a mass of 1543 MeV, a width of 134 MeV, and a πN branching fraction of 48%. This shows that it is possible to find fit parameters that roughly agree with the more complete models, but these results are of uncertain value given the strong model dependence.

The elastic πN amplitude (the upper two panels of Fig. 2) is more complicated, showing two structures overlapping in energy. The resonance $S_{11}(1650)$ couples strongly to πN with peaks at $W \sim 1.7$ GeV in Im(T) *and* at $W \sim 1.65$ GeV in Re(T). Although this rapid energy dependence is a clear resonant signal, there is also a nontrivial nonresonant amplitude which greatly distorts the typical Argand diagram. The energy dependence of $S_{11}(1535)$ is more complicated in πN elastic scattering because of the strong coupling to the ηN channel at its threshold ($W = 1.487$ GeV), which is within the resonant shape. This produces a cusp in the real part at threshold in addition to a peak in the imaginary part at ap-

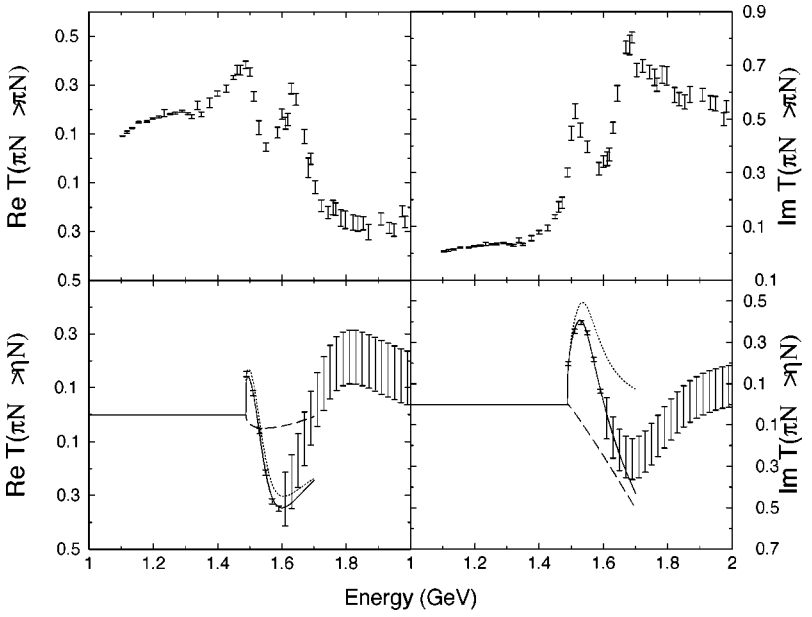

FIG. 2. Real parts (left panels) and imaginary parts (right panels) of $\pi N \to \pi N$ (upper panels) and $\pi N \to \eta N$ (lower panels) scattering amplitudes, T, in the S_{11} partial wave. The curves in the lower panels are the single-channel, one-resonance Breit-Wigner fit to these amplitudes described in the text. Dotted lines give the resonant, dashed lines the nonresonant, and solid lines the total scattering amplitude. Partial-wave amplitudes are shown with error bars.

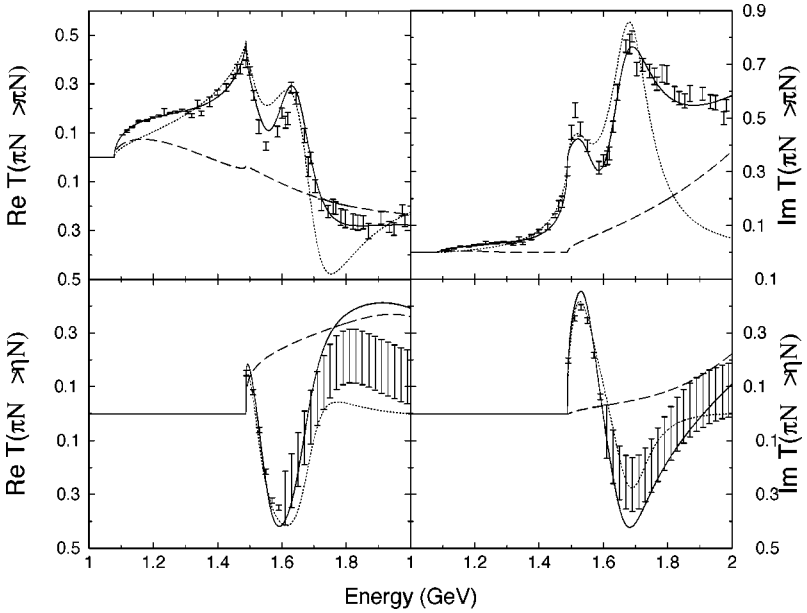

FIG. 3. Real parts (left panels) and imaginary parts (right panels) of $\pi N \rightarrow \pi N$ (upper panels) and $\pi N \rightarrow \eta N$ (lower panels) scattering amplitudes in the S_{11} partial wave. Dotted lines give the resonant, dashed lines the nonresonant, and solid lines the total scattering amplitude. Partial-wave amplitudes are shown with error bars. The resonant model used here is the two-resonance, two-channel CMB model described in the text, with nonresonant amplitudes described by distant poles.

proximately the resonance mass. Given this complicated structure, analyticity of the scattering amplitude and dispersive scattering effects can be expected to be most important for this state. For this reason, the elastic amplitude includes many of the important dynamical effects studied here.

After this somewhat pedagogical introduction, the main results of this work are now presented. The fits to the S_{11} partial-wave data for the T-matrix elements $T_{\pi N \rightarrow \pi N}$ and $T_{\pi N \rightarrow \eta N}$ for each resonant-non-resonant model are shown in Figs. 3–10. Unlike most previous papers studying N^* resonances, which show only the full amplitude, the nonresonant amplitude (with all resonant couplings set to zero) and the resonant amplitude (with all nonresonant couplings set to zero) are also shown here. The effective Breit-Wigner properties of the two resonances extracted from these fits are given in Tables I and II. Errors in the first four columns of results are determined from the fitting uncertainties only.

A common criterion in fits is the value of χ^2, given in the last row of the tables. A comparison of the two-channel fits shows that the lowest values of χ^2 are attained using the Breit-Wigner models with distant-poles background, the more theoretically sophisticated models are in between, and the Breit-Wigner models with polynomial background have the highest χ^2 values. Breit-Wigner models commonly have better fits because they are most often applied to study single-channel reactions, but are much more likely to have additional local minima close to the global minimum, reflecting the lack of theoretical constraints. The extra parameters required to get a good fit unfortunately obscure the physics results. The extraction of physically meaningful results for resonances depends more on the quality of the theoretical constraints placed on the fit than on the quality of the fit itself. In some cases the fit function is not as sharp as the data, e.g., the CMB and K-matrix model $\mathrm{Im}(T_{\pi N \rightarrow \pi N})$ ampli-

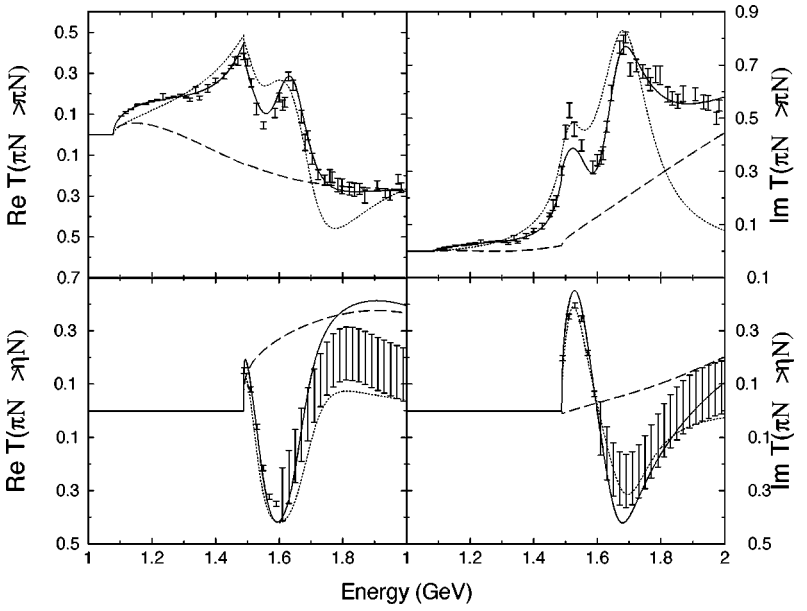

FIG. 4. Caption as in Fig. 3, except the resonant model used here is the K-matrix model described in the text, with nonresonant amplitudes described by distant poles.

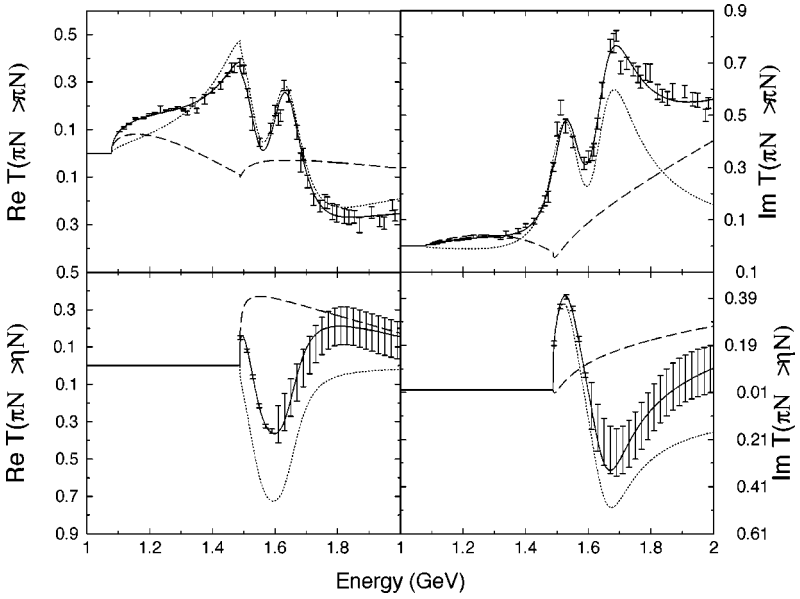

FIG. 5. Caption as in Fig. 3, except the resonant model used here is the Breit-Wigner model with nonrelativistic widths described in the text, with nonresonant amplitudes described by distant poles.

tudes with polynomial background, although this is not apparent from the total χ^2, which is summed over all data points. All models are able to match the shape of the cusp at ηN threshold in $\mathrm{Re}(T_{\pi N\to\pi N})$, since this is a property of interfering amplitudes and there are many possible solutions.

In the figures more detail is shown than is customary. For all models, the amplitudes are separated into resonant and nonresonant parts. The resonant amplitudes provide rapid energy fluctuations and a rough match to the data, especially for $\pi N\to\eta N$. The nonresonant amplitudes are generally smooth. However, analyticity constraints require a cusp at ηN threshold, a feature of all nonresonant amplitudes using distant-poles background. At first glance, the fits all look similar. More careful inspection reveals differences in the detailed balance between resonant and nonresonant amplitudes and in the channel coupling effects. One of the most striking features is seen in the $\pi N\to\pi N$ amplitude for the relativistic Breit-Wigner model with distant-poles background, Fig. 6. The imaginary part of the nonresonant amplitude is much larger at $W\sim 1.7$ GeV due to coupling to ηN than in the other models, a coupled channel effect. The resonant part of the amplitude is then smaller than in the other models and this model has a very small $B_{\eta N}$ for $S_{11}(1650)$.

The resonance parameters extracted using the various models are compared in Tables I and II. Variations among the results for the resonance masses, the full width, and the πN branching fraction are all significant given the estimated error bars of this study. The estimated errors would have to be much larger for the models to be in agreement. For reference, the result for the CMB model fitting two resonances with all open channels is shown in Table I. Note that the errors quoted for the CMB results include systematic errors from model uncertainties, and so are larger than the errors arising only from fitting uncertainties in the results of the present work. Many resonance parameters found in the two-channel CMB model are within the estimated errors of the full model.

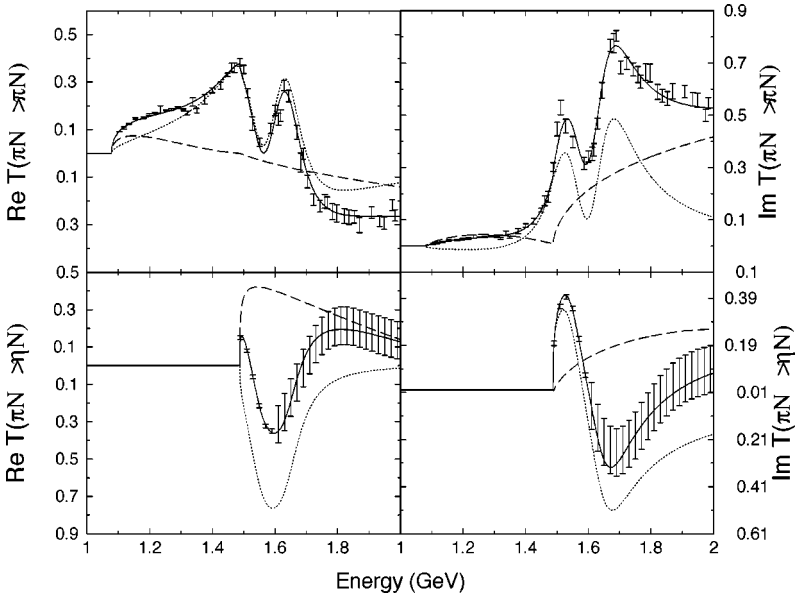

FIG. 6. Caption as in Fig. 3, except the resonant model used here is the Breit-Wigner model with relativistic widths described in the text, with nonresonant amplitudes described by distant poles.

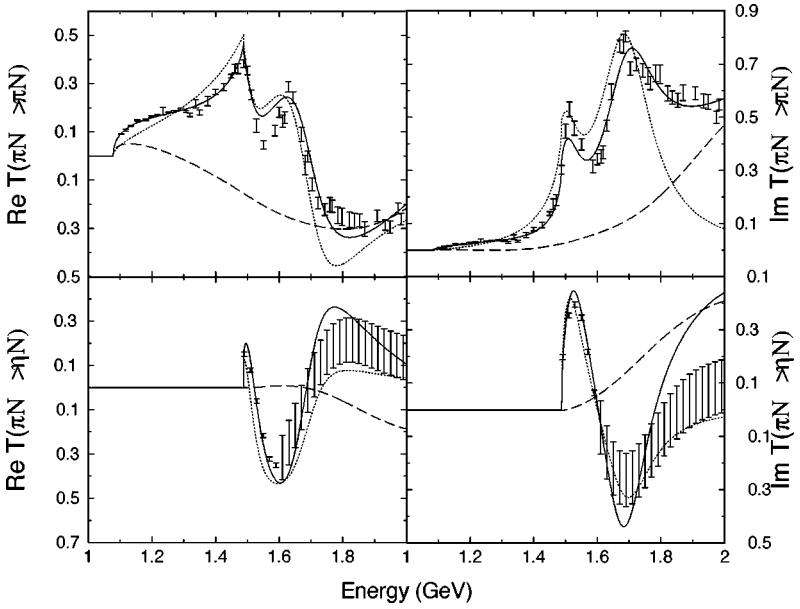

FIG. 7. Caption as in Fig. 3, except the resonant model used here is the two-resonance, two-channel CMB model described in the text, with nonresonant amplitudes described by polynomials.

The exception is the width of the $S_{11}(1650)$, where the full CMB-model value is larger than that of any of the other eight models. The full CMB-model fit apparently has a complicated interference between the second resonance and the channels that are excluded in the truncated versions. We also list the recommended physical parameters for these states from the Particle Data Group [10]. Almost all results are within the conservative estimated ranges they publish. It is interesting that although the results for the $S_{11}(1535)$ full width have significant variations using the different models studied here, the values are all in the lower part of the PDG estimated range. Similarly, the CMB and *K*-matrix results for $B_{\pi N}$ are all in the lower part of the PDG estimated range for that quantity.

Breit-Wigner models with relativistic and nonrelativistic resonance shapes are fitted separately and give almost identical results. Despite having the best fits, they give results that vary the most from the PDG values. Compared to the other results, the Breit-Wigner models have significantly lower mass, and smaller widths and πN branching fractions for $S_{11}(1650)$. This is more true for the fits using the polynomial background than for those using the distant-poles nonresonant amplitudes. Since the resonant peak in Im(T) smoothly blends in with the nonresonant background, the $S_{11}(1650)$ width is very sensitive to how this background is treated. Therefore, it is not surprising that the biggest discrepancies arise in this resonance property. Interference with the overlapping lower-energy state also has an important influence.

Comparisons between the CMB and *K*-matrix models are the most interesting. The full fit amplitudes in Figs. 3 and 4 are very similar. They even miss the sharp structure in the πN elastic amplitude at $W \sim 1.6$ GeV in the same way. At first glance the resonant and nonresonant amplitudes are also

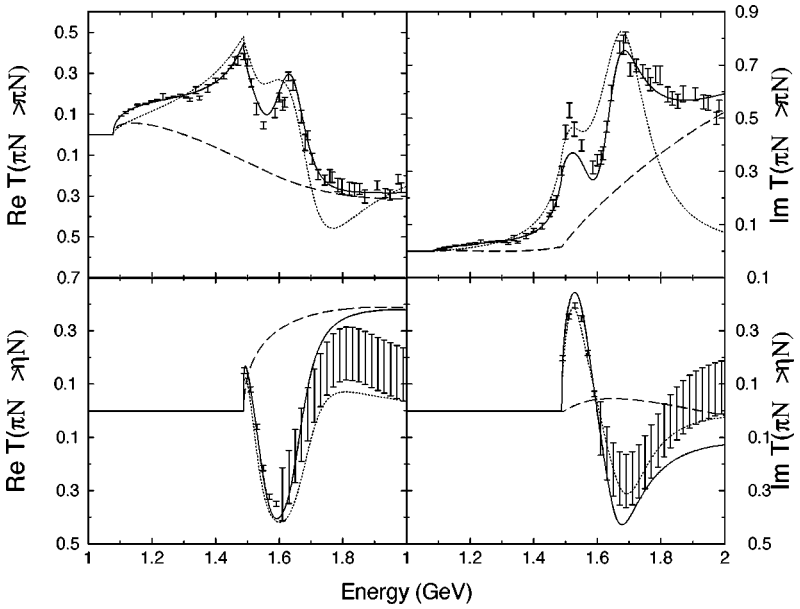

FIG. 8. Caption as in Fig. 4, except the resonant model used here is the *K*-matrix model described in the text, with nonresonant amplitudes described by polynomials.

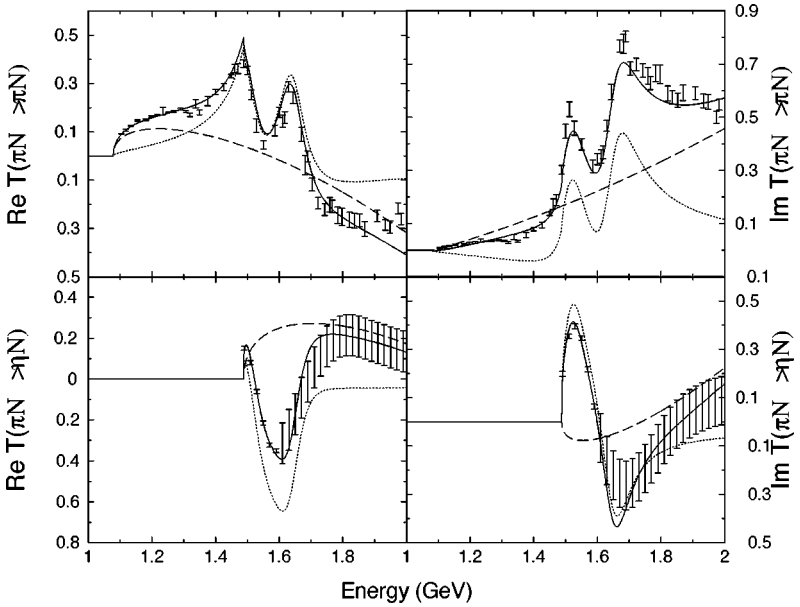

FIG. 9. Caption as in Fig. 3, except the resonant model used here is the Breit-Wigner model with nonrelativistic widths described in the text, with nonresonant amplitudes described by polynomials.

very similar, but the small difference in the shape of the imaginary elastic amplitude is the primary source of the differences in the extracted full width in the two models. The $S_{11}(1535)$ full width from the CMB model with distant-poles background is larger than for the *K*-matrix model with distant poles, and vice versa for the $S_{11}(1650)$ full width. For the error bars we derive, the difference in the full width is more significant than the difference in $B_{\pi N}$. This shows the interplay of the interfering resonances. On the other hand, the same two models with polynomial background (where the CMB model no longer satisfies analyticity) have very similar values for the full width. Interpretation of this result will be a key component of the discussion.

IV. DISCUSSION

A variety of empirical models were used to fit partial-wave amplitudes (the input "data") for a carefully chosen problem, the S_{11} partial wave and its two most important channels, πN and ηN. This partial wave is interesting because of the physics interest in the S_{11} resonances and the large uncertainty in their properties as reported by the PDG [10]. By using identical input amplitudes and fitting strategies, we have made the *first objective comparison* of N^* resonance extraction models. Four different resonance models (CMB, *K* matrix, and Breit-Wigner with nonrelativistic and relativistic widths), and two different empirical models for the nonresonant amplitude (distant poles and polynomial) are employed. These models are in regular use for the extraction of hadronic properties. It should be emphasized that the four resonance models have almost identical amplitudes for isolated resonances. The primary differences among the models come from the way the dynamics of resonance interference, multichannel effects, and nonresonant amplitudes are treated. Although resonance models of widely varying quality are employed, the nonresonant models are both rather empirical. However, this partial wave in these channels has nonresonant

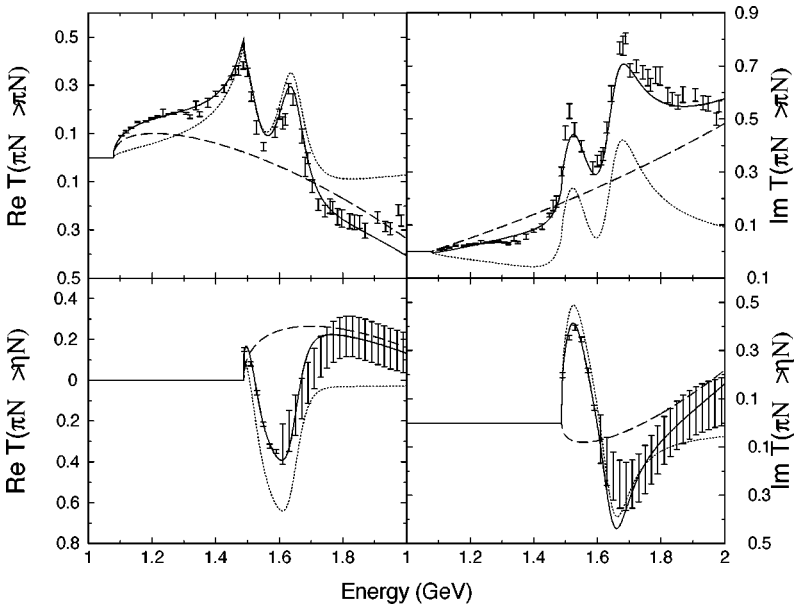

FIG. 10. Caption as in Fig. 3, except the resonant model used here is the Breit-Wigner model with relativistic widths described in the text, with nonresonant amplitudes described by polynomials.

TABLE I. Results for resonance parameters from fits to the T-matrix elements for $\pi N \to \pi N$, ηN in the S_{11} partial wave, using the CMB, K-matrix, and Breit-Wigner (BW) models described in the text. The third to last column shows the results of a fit including $\pi N \to \pi N$, ηN, ρN, $\pi\Delta$, σN, and πN^* partial-wave amplitudes [9]. The next to last column shows results for a fit of the πN data and $\gamma N \to \pi N$, ηN data [21], and the last column shows the range in the central values and estimated values from the PDG [10]. Nonresonant contributions to the T matrix are described in terms of distant poles in all cases. Since the primary results of this work come from a two-channel model, only the branching fraction to πN is given, since $B_{\eta N}=1-B_{\pi N}$. The last row gives the χ^2 per data point of each fit.

Model	CMB	K matrix	$BW_{n.r.}$	BW_{rel}	CMB all πN	CMB all πN, γN	PDG
$S_{11}(1535)$							
Mass (MeV)	1539±1	1533±1	1549±2	1558±1	1547±3	1539±5	1520 −1555(1535)
Width (MeV)	135±4	115±3	142±9	143±4	131±19	122±20	100−200(150)
$B_{\pi N}$ (%)	29±1	34±1	67±5	67±1	34±4	39±5	35−55
$S_{11}(1650)$							
Mass (MeV)	1682±1	1685±2	1648±5	1637±2	1690±12	1684±15	1640 −1680(1650)
Width (MeV)	144±3	190±5	147±10	145±4	227±40	227±58	145−190(150)
$B_{\pi N}$ (%)	80±1	77±1	74±5	79±1	75±3	75±3	55−90
χ^2/N	3.8	3.7	1.5	1.9	3.6	5.6	

amplitudes which are comparatively small. Since the nonresonant amplitudes have a smooth energy dependence, their influence on the extracted resonance parameters should be small. The main purpose of this work is to study the model dependence of the extraction of S_{11} properties (mass, width, and πN branching fraction) in a case where overlapping resonances, multichannel effects, and analyticity constraints are all expected to be important.

The models used here can be put in order according to the theoretical constraints employed. The CMB model with distant-poles background satisfies multichannel unitarity and constraints from analyticity, and handles resonance-resonance quantum mechanical interference well. In fact, the CMB model includes the most complete resonance propagation effects of any of the existing models. The K-matrix model used here does not satisfy analyticity constraints, and leaves out rescattering dynamics present in the CMB model. The Breit-Wigner models used here satisfy essentially no theoretical constraints. However, unitary Breit-Wigner models [12] and K-matrix models that satisfy analyticity constraints [18] have been developed.

The large range of properties for the two lowest-energy S_{11} resonances in the Review of Particle Properties [10] is also found here. This is evidence that much of the uncertainty in the PDG estimates of S_{11} properties comes from model dependence, since the same input amplitudes are used in every fit. No evidence is found for a third S_{11} state in the energy range studied. Some of the Breit-Wigner models have the best fits to the data, but this is due to the flexibility of these models rather than an ability to describe the underlying dynamics. Arbitrary adjustments must be employed in order to obtain good fits to the data. The empirical phases between the resonances provide a simple way to adjust the resonance-resonance interference at the cost of obscuring the physics output. As a result, the physical properties of the $S_{11}(1650)$ determined with the Breit-Wigner models are very different than with the other models.

The models with the strongest theoretical constraints, the CMB and K-matrix models with distant-poles background, provide better agreement with each other and with the CMB fits to a much larger set of reactions [9,21]. One major result of the present work is the differences between CMB and K-matrix models found in a situation where their differences should be the largest. The extent of the disagreement cannot

TABLE II. Caption as in Table I, except nonresonant contributions to the T matrix are described in terms of polynomials.

	Model	CMB	K matrix	$BW_{n.r.}$	BW_{rel}
$S_{11}(1535)$	Mass (MeV)	1526±2	1533±1	1539±2	1538±2
	Width (MeV)	112±6	119±3	130±6	130±6
	$B_{\pi N}$ (%)	30±2	33±1	39±1	38±1
$S_{11}(1650)$	Mass (MeV)	1688±2	1682±2	1648±2	1647±2
	Width (MeV)	193±6	184±5	109±5	109±5
	$B_{\pi N}$ (%)	78±2	75±1	51±1	51±1
	χ^2/N	5.0	3.9	5.0	5.0

be simply stated. For the error bars given for the input amplitudes and those determined in our fits, the difference between the $S_{11}(1535)$ mass and full width for the CMB and *K*-matrix models with distant poles is significant. This is an important measure of the difference in these two models.

Other considerations could contribute to these differences. The estimated errors quoted in the partial-wave amplitude fits have a direct effect on the values quoted here. It is possible that the errors in the partial-wave amplitudes are understated due to a lack of understanding of the model dependence. Although a more sophisticated nonresonant amplitude could be required, the smoothness of these amplitudes in all models argues against this. Each model has problems that are likely due to the truncated channel space employed. The most obvious problem is with the width of $S_{11}(1650)$. About 20% of the overall strength that was supposed to go to channels other than πN and ηN has to be included somewhere in the smaller channel space.

In the context of the small but important test case chosen for this study, the results of the CMB and *K*-matrix model fits are found to have small, but potentially important differences. Since the CMB model is better constrained theoretically, the resonance properties extracted using this model should be preferred when there is reason to doubt other models. A possible conclusion could be that this proves that the constraints provided by analyticity, a superior treatment of rescattering, and an improved treatment of resonance interference are important in this case. From the present limited comparison, such a conclusion is likely premature. This issue requires further study, particularly from the theoretical side.

We should note that many N^* states will not be obscured by strong threshold effects and will not have strong interference with other states of the same angular momentum and parity. The simplified dynamics of the *K*-matrix model then give it the practical advantage of a simpler and more stable path to a good fit to the partial-wave amplitudes. Proper use of this model in the analysis of N^* data is unlikely to give results that are badly incorrect. For resonances with a larger number of open channels, the interaction of the nonresonant and resonant amplitudes can be much more complicated and simplified fitting can give erroneous results.

The primary result of this paper is that even in a small multichannel problem, dynamics are important. Since Breit-Wigner models have very few theoretical constraints, *ad hoc* parameters are required to fit real data such as those of the two-channel problem studied here. We therefore suggest that consideration of these issues be part of any attempt to determine global recommendations for baryon resonance properties.

ACKNOWLEDGMENTS

This research was supported by the U.S. Department of Energy under Contract DE-FG02-86ER40273 (A.K., S.C.), and by the National Science Foundation under Grant No. PHY-0140116 (S.D.).

[1] N. Isgur and G. Karl, Phys. Rev. D **18**, 4187 (1978); S. Capstick and N. Isgur, *ibid.* **34**, 2809 (1986); L. Y. Glozman and D. O. Riska, Phys. Rep. **268**, 263 (1996); L. Y. Glozman, Z. Papp, and W. Plessas, Phys. Lett. B **381**, 311 (1996); see also the review by S. Capstick and W. Roberts, Prog. Part. Nucl. Phys. **45**, S241 (2000), and references therein.

[2] T. Inoue, E. Oset, and M. J. Vicente Vacas, Phys. Rev. C **65**, 035204 (2002); J. Nieves and E. Ruiz Arriola, Phys. Rev. D **64**, 116008 (2001).

[3] M. Göckeler, R. Horsley, D. Pleiter, P. E.L. Rakow, G. Schierholz, C. M. Raynard, and D. Richards, Phys. Lett. B **352**, 63 (2002).

[4] S. Dong, T. Draper, I. Horvath, F. X. Lee, K. F. Liu, N. Mathur, and J. B. Zhang, LANL preprint, hep-ph/0306199.

[5] J. Chizma and G. Karl, Phys. Rev. D **68**, 054007 (2003).

[6] Richard A. Arndt, Igor I. Strakovsky, Ron L. Workman, and Marcello M. Pavan, Phys. Rev. C **52**, 2120 (1995).

[7] G. Höhler, F. Kaiser, R. Koch, and E. Pietarinen, *Handbook of Pion-Nucleon Scattering* (Fachinform. Zentr., Karlsruhe, 1979).

[8] B. Krusche, Nimai C. Mukhopadhyay, J. F. Zhang, and M. Bennmerrouche, Phys. Lett. B **397**, 171 (1997).

[9] T. P. Vrana, S. A. Dytman, and T.-S. H. Lee, Phys. Rep. **328**, 181 (2000).

[10] Particle Data Group, K. Hagiwara *et al.*, Phys. Rev. D **66**, 010001 (2002).

[11] R. D. Baker *et al.*, Nucl. Phys. **156**, 93 (1979).

[12] D. Drechsel, O. Hanstein, S. S. Kamalov, and L. Tiator, Nucl. Phys. **A645**, 145 (1999).

[13] G. Penner and U. Mosel, Phys. Rev. C **66**, 055211 (2002).

[14] A. M. Green and S. Wycech, Phys. Rev. C **55**, R2167 (1997).

[15] M. Batinic, I. Slaus, A. Svarc, and B. M. K. Nefkens, Phys. Rev. C **51**, 2310 (1995).

[16] R. E. Cutkosky, C. P. Forsyth, R. E. Hendrick, and R. L. Kelly, Phys. Rev. D **20**, 2839 (1979).

[17] D. M. Manley, Int. J. Mod. Phys. A **18**, 441 (2003).

[18] R. S. Longacre, T. Lasinski, A. H. Rosenfeld, G. Smadja, R. J. Cashmore, and David W.G.S. Leith, Phys. Rev. D **17**, 1795 (1978).

[19] R. G. Moorhouse, H. Oberlack, and A. H. Rosenfeld, Phys. Rev. D **9**, 1 (1974).

[20] S. U. Chung, J. Brose, R. Hackmann, E. Klempt, S. Spanier, and C. Strassburger, Ann. Phys. **4**, 404 (1995).

[21] T. Vrana, S. A. Dytman, and T.-S. H. Lee (unpublished).